Eur. Phys. J. Plus (2022) 137:1340
https://doi.org/10.1140/epjp/s13360-022-03530-9

THE EUROPEAN PHYSICAL JOURNAL PLUS

Regular Article

Lattice deformation and potential effects on linear and nonlinear optical properties of doped SiGe quantum dot encapsulated in Si matrix

Varsha[1,2], K. Lakaal[3,4], M. Kria[3,4], J. El Hamdaoui[3,4], V. Prasad[5,a], E. Feddi[3,6], D. Laroze[7], L. M. Pérez[8], M. E. Mora Ramos[9,b]

[1] Department of Physics and Astrophysics, University of Delhi, Delhi 110007, India
[2] Department of Physics, Kalindi College, University of Delhi, Delhi 110008, India
[3] Group of Optoelectronic of Semiconductors and Nanomaterials, ENSAM, Mohammed V University in Rabat, Rabat, Morocco
[4] Laboratory of Condensed Matter and Interdisciplinary Sciences (LaMCScI), Faculty of Sciences Rabat, Mohammed V University in Rabat, Morocco V University in Rabat, Rabat, Morocco
[5] Department of Physics, Swami Shraddhanand College, University of Delhi, Delhi 110036, India
[6] Institute of Applied Physics, Mohammed VI Polytechnic University, Lot 660, Hay Moulay Rachid, Ben Guerir 43150, Morocco
[7] Instituto de Alta Investigación, CEDENNA, Universidad de Tarapacá, Casilla 7 D, Arica, Chile
[8] Departamento de Física, FACI, Universidad de Tarapacá, Casilla 7 D, Arica, Chile
[9] Facultad de Ciencias, Universidad Autónoma del Estado de Morelos, Ave. Universidad 1001, CP 62209 Cuernavaca, Morelos, Mexico

Received: 31 July 2022 / Accepted: 22 November 2022
© The Author(s), under exclusive licence to Società Italiana di Fisica and Springer-Verlag GmbH Germany, part of Springer Nature 2022

Abstract Electron states in spheroid $Si_{0.7}Ge_{0.3}$ quantum dots are investigated taking into account the presence of a donor impurity atom and a weak external electromagnetic laser field. The conduction band confining profile along the radial direction is modelled by a parameterized exponential potential. Based on the calculated inter-state transition energies, the nonlinear optical responses associated with light absorption, relative refractive index change, and second and third harmonics generation are evaluated and discussed. Results are reported considering different positions of the donor center in the dot as well as for different values of the exponential potential parameter. When the impurity is shifted to different position, the polarisation changes inside the dot and hence the energy and wave function of the system. The change of impurity position from center to edge of the dot causes redshift whereas the increase in potential parameter causes blueshift.

1 Introduction

Research and fabrication of optoelectronic devices underwent what may be called as a revolution after the proposal and development of semiconductor quantum dots (QDs) in 1980s [1, 2]. Progress on the subject has been reviewed in several occasions throughout the years [3–7]. Thanks to advanced epitaxial growth, beam lithography and reactive etching procedures, it has been possible to fabricate different kind of nanostructures with precise control of the wetting layer. Such a procedure is not exempt of technological challenges posed, in many cases, by the physical nature of the involved materials. Accordingly, lattice mismatch gives rise to strain, which conditions the geometry of obtained QD systems—with or without a wetting layer (WL)—as it has been revealed by accurate imaging. Thus, QD with cylindrical, conical, pyramidal, hemispherical, disc, lens, ring, dome, oblate (or semi-oblate) and prolate shapes have been dealt with either experimentally or from the theoretical point of view [8–17].

SiGe/Si QDs have attracted attention not only due to their optical properties, such as photoluminescence in the visible range [18], but also mostly in relation with their promising features with regard to qubit hosting, pointing at core applications for quantum computing [19–26]. The field of nonlinear optics is growing due to its vast applications like second harmonic generation, third harmonic generation, etc. [27] The nonlinear response of the hetero-structure arises in the anisotropic medium where the polarization is expressed as a power series where the contribution from nonlinear terms arises only when the field strength of the applied field is high. These effects were observed after the invention of the laser which is a highly coherent source of high intensity so the contribution of the nonlinear terms increases. Here, we investigate SiGe/Si QDs from the perspective of their nonlinear optical response. In particular, we assume the presence of ionized, hydrogenic-like, impurity atom and model the electron confinement with an attractive power exponential potential function. In this way, we theoretically evaluate the coefficients of optical absorption, relative refractive index change, second harmonics generation (SHG), and third harmonics generation (THG); all of them are related with transitions between allowed electron states in the system, influenced by the electrostatic interaction with the Coulombic center.

[a] e-mail: vprasad@ss.du.ac.in (corresponding author)
[b] e-mail: memora@uaem.mx

Published online: 13 December 2022

It is worth mentioning that calculations of these optical quantities in QDs—including Si/SiGe ones—have also been put forward in several works by different researchers. Optical absorption coefficient (OAC) and relative change of refractive index coefficient (RIC) is reported in references [17, 28–32]. Evaluation of SHG can be found in the articles [17, 32–35], while that of THG appears in references [17, 35, 36]. The main goal of reporting these studies of the literature is to mention the importance of these works as these quantum hetero-structures in different dimensions can be used for a variety of purposes like hetero-structures lasers, solar cells, LED, etc., as indicated by the authors.

Previously, the authors have also investigated the optical properties for SiGe/Si semi-oblate and prolate QDs with and without electric field with wetting layer effect [17, 37]. Using finite element method, the optical properties of a spheroidal-shaped SiGe/Si QD with hydrogenic impurity in the presence of power-exponential potential are explored in the present work.

In real life, instead of an abrupt gap, the genuine hetero-structure admits a graded variation of gap energy that resembles stairs, allowing different potentials to imitate these stairs. One of these is the power-exponential potential. Utilizing the power-exponential potential, Lin and Ho investigated the photoionization of atoms contained within cages [38]. The choice of the potential gives cage shell boundaries a flexibility to confine charge carriers. Jahan et al. [39] using the power-exponential potential model with the steepness parameter p, the impact of the confinement potential's shape on the electrical, thermodynamic, magnetic, and transport properties of a GaAs QD is investigated. Xie uses power exponential potential to investigate the photoionization cross section of a donor in QDs [40]. In this work, we shall focus our attention on the effect over transition energies and, thus, on the optical coefficients, of changing value for the exponent index of the confining potential, acting inside the core and WL regions of the SiGe/Si QD structure, and its competition with the Coulomb term. Article organization is as follows: Section II contains details of the theoretical framework. Section III is devoted to present and discuss the obtained results, and in Section IV, we present the corresponding conclusions.

2 Theory

We have taken system of $Si_{1-x}Ge_x$ spheroidal QD within Si matrix deposited on Si wetting layer with $x = 30\%$, with an ionized donor impurity at the center. $Si_{1-x}Ge_x$ is more like Si material for $x \prec 0.85$, x is the composition of Ge material, here we have taken $x = 0.3$.

Figure 1 shows the SiGe QD embedded in Si matrix. From the potential profile shown in Fig. 2, we see that for small values of P (less than 1), the potential is very sharp at center and drops rapidly as one moves from the center. This behavior gives an entire new regime of the potential to explore which is not studied earlier. The eigen-energies and corresponding wave functions are solution of the Schrödinger equation:

$$\frac{-\hbar^2}{2}\nabla\left[\frac{1}{m_i^*(r)}\nabla\psi(r)\right] + V_w^e(r)\psi(r) + V_c(r)\psi(r) + V_s\psi(r) = E\psi(r) \tag{1}$$

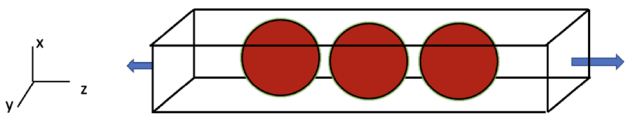


Fig. 1 Spherical QD of SiGe embedded in Si matrix

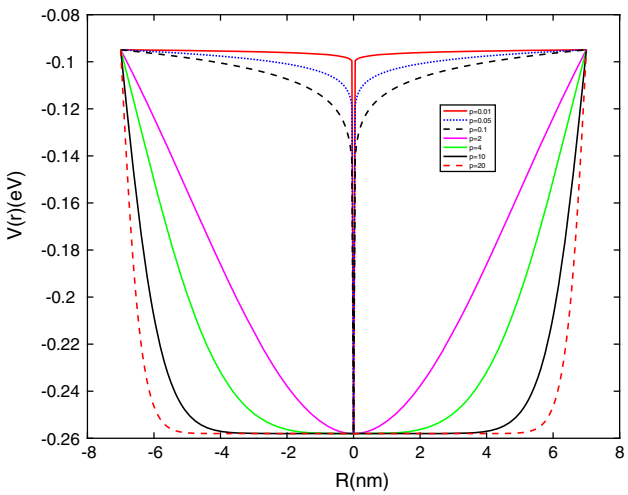


Fig. 2 Power exponential potential profile for different P values

where $\psi(r)$ and E are the wave functions and the energy levels respectively. m_i^* is the position dependent effective mass of the electron, i.e., different for matrix and QD region given as:

$$m_i^* = \begin{cases} m_{SiGe}^* & \text{inside the core and the WL} \\ m_{Si}^* & \text{otherwise} \end{cases} \tag{2}$$

The effective mass of electron for Si, along longitudinal (m_l) is $0.92m_0$ and along transverse (m_t) is equal to $0.19\ m_0$ and for Ge, $m_l = 1.64\, m_0$ and $m_t = 0.082\, m_0$. The dielectric strength as a composition of x is given by $\epsilon(x) = 11.9\ (1 + 0.35\ x)$.

For $x < 0.85$, the $Si_{1-x}Ge_x$ alloys are considered as Si-like material. The effective mass of electron is calculated using the formula:

$$m_e^* = \frac{3}{\frac{1}{m_l} + \frac{2}{m_t}} \tag{3}$$

Therefore, the effective mass for SiGe for being Si-like is taken equal to Si material, i.e., $m_{SiGe}^* = 0.26\, m_0$. The variation of effective mass with temperature is given as

$$m_e^*(T) = \frac{m_0}{1 + \frac{C_i}{E_g(T)}} \tag{4}$$

where $C_i = 3.19$ eV.

The expression for bandgap dependence on temperature with the material composition is given by:

$$E_g^{SiGe}(T) = E_g^{Si}(0).(1-x) + E_g^{Ge}(0).x + C_g.(1-x)x - \frac{\alpha.T^2}{\beta + T} \tag{5}$$

where $E_g^{Si}(0) = 1.166$ eV, $E_g^{Ge}(0) = 0.7437$ eV, $C_g = -0.4$ eV, $\alpha = 4.73 \times 10^{-4}$ eV/K and $\beta = 636$ K.

The confining potential energy $V_w^e(r)$ and the coulombic potential $V_c(r)$ is given by:

$$V_w^e(r) = \begin{cases} -V_0 exp(-(\frac{r}{R})^P) & \text{inside the core and the WL} \\ 0 & \text{otherwise} \end{cases} \tag{6}$$

Here, P can take any integral values. V_s is the strain potential induced by lattice mismatch [41]. The parameters P determine the shape of the confinement potential and provide a measurement of the steepness of the potential at the QD boundary. V_0 denotes the depth of the potential which is taken as band offset between the two materials, R provides a measure of the potential's range and thus reflects the effective confinement length or size of the QD. The potential is softer (harder) depending on the size of the parameter P is smaller (larger). We have chosen R in such a way so that the charge carriers are confined in the well.

$$V_s = \begin{cases} -D_0 & \text{inside the core and the WL} \\ 0 & \text{otherwise} \end{cases} \tag{7}$$

where $D_0 = a_v^{Si_{1-x}Ge_x}\varepsilon_{\parallel} \pm b_v^{Si_{1-x}Ge_x}\varepsilon_{\parallel\perp}$. Here, (+) sign is for light hole and (−) sign is for heavy hole. $a_v^{Si_{1-x}Ge_x}$ and $b_v^{Si_{1-x}Ge_x}$ are the deformation potential parameters of $Si_{1-x}Ge_x$ and $\varepsilon_{\parallel}$ and $\varepsilon_{\parallel\perp}$ is given as [41]

$$\varepsilon_{\parallel} = \frac{a_{Si} - a_{Si_{1-x}Ge_x}}{a_{Si_{1-x}Ge_x}}; \qquad \varepsilon_{\perp} = \varepsilon_{\parallel}\left(-2\frac{C_{12}^{Si_{1-x}Ge_x}}{C_{11}^{Si_{1-x}Ge_x}}\right); \qquad \text{and} \quad \varepsilon_{\parallel\perp} = \varepsilon_{\parallel} - \varepsilon_{\perp} \tag{8}$$

where $a_{Si_{1-x}Ge_x}$ (a_{Si}) is lattice constant of $Si_{1-x}Ge_x$ (Si). $C_{11}^{Si_{1-x}Ge_x}$ and $C_{12}^{Si_{1-x}Ge_x}$ are the elastic moduli of $Si_{1-x}Ge_x$. The value of deformation potential parameters, lattice constant and elastic moduli are given in Table 1. In addition, the Coulombic energy term, $V_c(r)$, is

$$V_c(r) = \begin{cases} -\frac{e^2}{4\pi\epsilon(r)\vec{\xi}} & \text{inside the core and the WL} \\ 0 & \text{otherwise} \end{cases} \tag{9}$$

Here, $V_0 = E_g(Si) - E_g(Si_{1-x}Ge_x)$, $\vec{\xi} = |\vec{r} - \vec{Z}|$, and $r = \sqrt{x^2 + y^2 + z^2}$, where Z is the position of impurity. When impurity is at center, Z=0 and for non-center position of impurity $Z \neq 0$. We have taken different cases in our study as shown in results. $\vec{\xi}^2 = \vec{r}^2 + \vec{Z}^2 - 2Zrcos\theta$ which implies $\vec{\xi} = \sqrt{r^2 + Z^2 - 2Z(rcos\theta)}$, as we know that $z = (rcos\theta)$, therefore $\vec{\xi} = \sqrt{((x^2 + y^2 + z^2) + Z^2) - 2Zz}$. The dielectric constant in the system varies with position as

$$\epsilon(r) = \frac{\epsilon_{in}}{1 + \frac{r}{R}\left(\frac{\epsilon_{in}}{\epsilon_{out}} - 1\right)} \tag{10}$$

where R is the size of QD. The analytical solution of the Schrödinger equation for these geometrical shapes is arduous. We have used the finite element method with the proper choice of boundary conditions as per the physical condition to study our system as shown in Fig. 1. Whenever an electromagnetic field $\mathcal{E}(t) = \mathcal{E}_0 e^{j(\omega t)} + \mathcal{E}_0 e^{-j(\omega t)}$ with frequency ω interacts with the system, there

Table 1 Physical parameters of *Si*, *Ge*, and $Si_{0.7}Ge_{0.3}$

	m_e^*/m_0	ε	E_g (eV)	$a(A^\circ)$	C_{11} (10^{12} dyne/cm^{-2} or MPa)	C_{12} (MPa)	a_v (eV)	b_v (eV)
Si	0.26	11.9	1.12	5.431	1.675	0.650	0	2.33
Ge	0.12	16	0.66	5.658	1.315	0.494	0	2.08
$Si_{0.7}Ge_{0.3}$	0.26	13.15	0.89	5.489	1.557	0.599	0	2.25

are changes in the polarization which has both linear and nonlinear components as the electric field can be expanded using power series [27]. We recall that the electronic polarization of the nth order on $\mathcal{E}(t)$ can be expressed as [45]:

$$P^n \equiv \varepsilon_0[\chi^{(1)}\mathcal{E}(t) + \chi^{(2)}\mathcal{E}^2(t) + \chi^{(3)}\mathcal{E}^3(t) + ...]., \tag{11}$$

where ε_0 is the permittivity of the free space, $\chi^{(1)}$, $\chi^{(2)}$, $\chi^{(3)}$ are the linear, second-order and third-order susceptibilities, respectively, and $\mathcal{E}(t)$, $\mathcal{E}^2(t)$, $\mathcal{E}^3(t)$ linear, second-order and third-order optical electric field, respectively.

In order to analyze the optical properties, we use the well-known formalism based on the density matrix approach [42–44] which allows us to determine, the linear and nonlinear (third-order) contributions to the dielectric susceptibility. From such an information, it is possible to derive the expressions needed to evaluate the OACs and RICs.

Then, total OAC is given as:

$$\alpha(\omega, I) = \alpha^{(1)}(\omega) + \alpha^{(3)}(\omega, I), \tag{12}$$

where $\alpha^{(1)}$ is given by,

$$\alpha^{(1)}(\omega) = \omega\sqrt{\frac{\mu}{\varepsilon}}\frac{\hbar\,\Gamma_{\rm if}\,|M_{\rm fi}|^2\,\sigma}{(E_{\rm fi} - \hbar\omega)^2 + (\hbar\,\Gamma_{\rm if})^2} \tag{13}$$

and the expression of third order AC is written as:

$$\begin{aligned}\alpha^{(3)}(\omega, I) = &-\omega\sqrt{\frac{\mu}{\varepsilon}}\left(\frac{I}{2\varepsilon_0 n_{\rm r} c}\right)\frac{4\sigma\hbar\Gamma_{\rm if}|M_{\rm fi}|^4}{\left[(E_{\rm fi} - \hbar\omega)^2 + (\hbar\Gamma_{\rm if})^2\right]^2}\\ &\left[1 - \frac{(M_{\rm ff} - M_{ii})^2}{4|M_{\rm fi}|^2}\left\{\frac{3E_{\rm fi}^2 - 4\hbar\omega E_{\rm fi} + \hbar^2\left(\omega^2 - \Gamma_{\rm if}^2\right)}{E_{\rm fi}^2 + (\hbar\Gamma_{\rm if})^2}\right\}\right]\end{aligned} \tag{14}$$

In these conditions, the RICs written as

$$\frac{\Delta n(\omega)}{n_{\rm r}} = \frac{\Delta n^{(1)}(\omega)}{n_{\rm r}} + \frac{\Delta n^{(3)}(\omega)}{n_{\rm r}} \tag{15}$$

where

$$\frac{\Delta n^{(1)}(\omega)}{n_{\rm r}} = \frac{1}{2\varepsilon_0 n_{\rm r}^2}\frac{\sigma|M_{\rm fi}|^2(E_{\rm fi} - \hbar\omega)}{(E_{\rm fi} - \hbar\omega)^2 + (\hbar\Gamma_{\rm if})^2} \tag{16}$$

and

$$\begin{aligned}\frac{\Delta n^{(3)}(\omega, I)}{n_{\rm r}} = &-\frac{\mu c I\sigma|M_{\rm fi}|^4}{\varepsilon_0 n_{\rm r}^3}\frac{(E_{\rm fi} - \hbar\omega)}{\left[(E_{\rm fi} - \hbar\omega)^2 + (\hbar\Gamma_{\rm if})^2\right]^2}\left[1 - \frac{(M_{\rm ff} - M_{ii})^2}{4|M_{\rm fi}|^2\left(E_{\rm fi}^2 + (\hbar\Gamma_{\rm if})^2\right)}\right.\\ &\left.\times\left\{E_{\rm fi}(E_{\rm fi} - \hbar\omega) - (\hbar\Gamma_{\rm if})^2 - (\hbar\Gamma_{\rm if})^2\frac{(2E_{\rm fi} - \hbar\omega)}{(E_{\rm fi} - \hbar\omega)}\right\}\right]\end{aligned} \tag{17}$$

where $E_{\rm fi} = E_{\rm f} - E_{\rm i}$ denotes the energy transition between an initial state (i) and a final state (f) $M_{\rm fi} = e < \Psi_f|x|\Psi_i >$ is the electric dipole moment of the transition from the i states to f states . We recall that the parameters used above are: c for the speed of light in a vacuum, and σ_s is the electron density related to the occupied volume by the relation. I is the intensity of the incident electromagnetic radiation, ω is the angular frequency of the laser radiation, μ is the permeability of the system, n_r is the relative refractive index of semiconductor, ε_0 is the permittivity of free space. $\Gamma_{\rm fi}$ is the line width and also recognized as the non-diagonal matrix element defined as the inverse of the relaxation time $\tau_{\rm fi}$ and known as the relaxation rate of initial and final states.

3 Results and discussion

To perform the theoretical investigation describe in the previous section, we have considered the following set values for the main input parameters—unless mentioned otherwise: $P = 1$, $Z = 0$, $R = 7$ nm, $T = 300$ K. In addition, the value of refractive index is $n_r = 3.55$ ($\varepsilon/\varepsilon_0 = 13.05$), while evaluation of the corresponding band alignment leads to $V_0 = 258$ meV. We are also assuming an electron volume density $\sigma_v = 2 \times 10^{22}$ cm^{-3}, a transition rate $\Gamma_{10} = 0.38$ ps^{-1}, and a value of incident—resonant—radiation $I = 2 \times 10^7$ w/m^2.

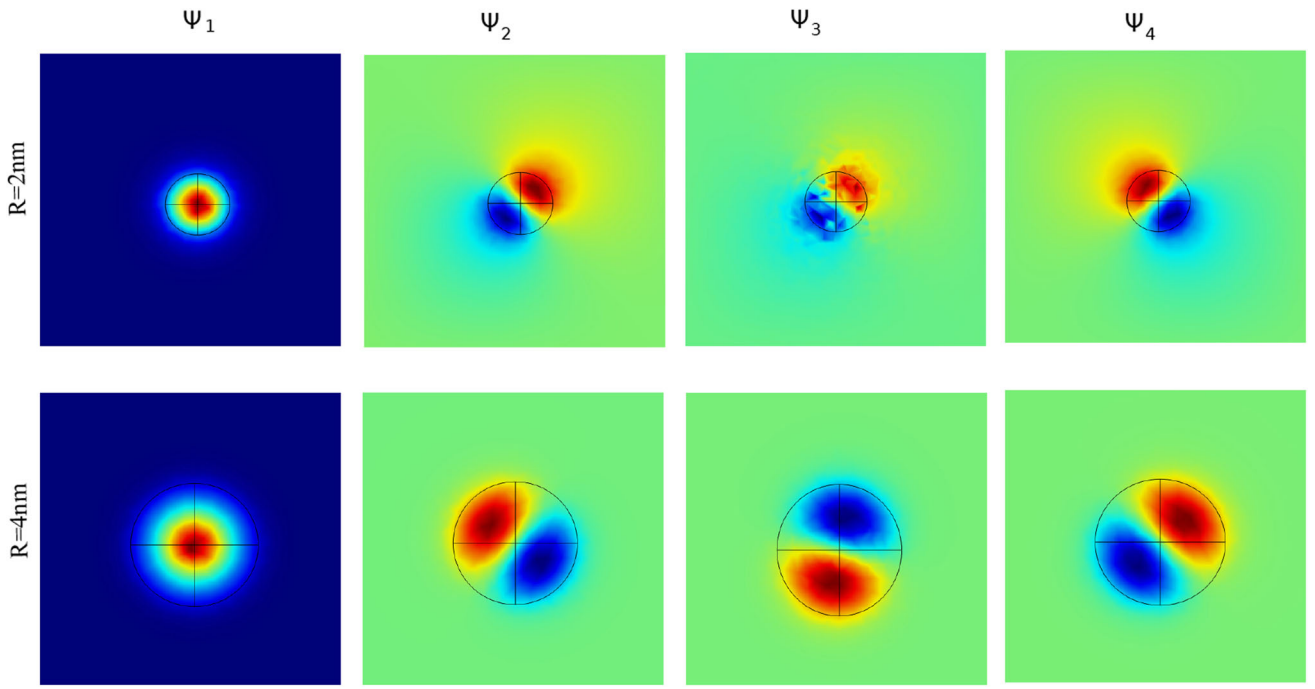


Fig. 3 Wave function of the four low-lying states for two different values of quantum dot radius, when the impurity is assumed to be located at the center of sphere ($Z = 0$) with $P = 1$. Red colors indicate maximum values, while blue ones correspond to minimum values

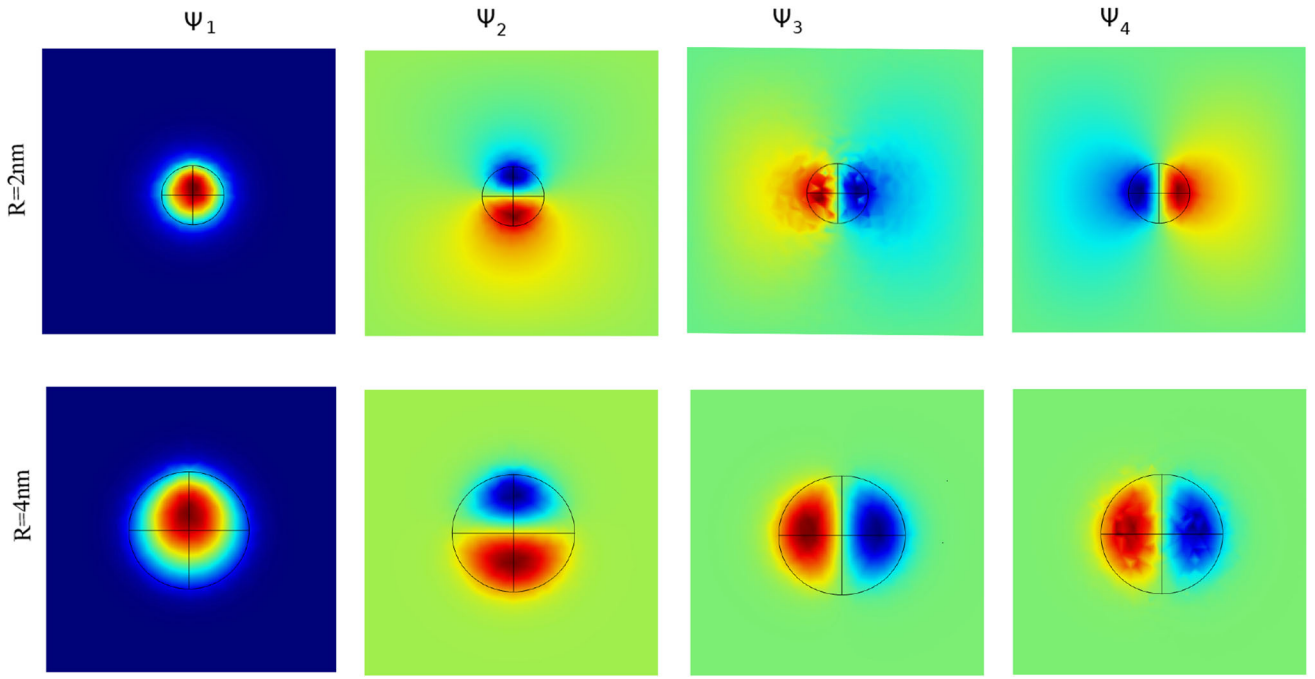


Fig. 4 Wave function of the four low-lying states for two different values of quantum dot radius, when the impurity is assumed to be located on the edge of sphere ($Z = R$) with $P = 1$. Red colors indicate maximum values, while blue ones correspond to minimum values

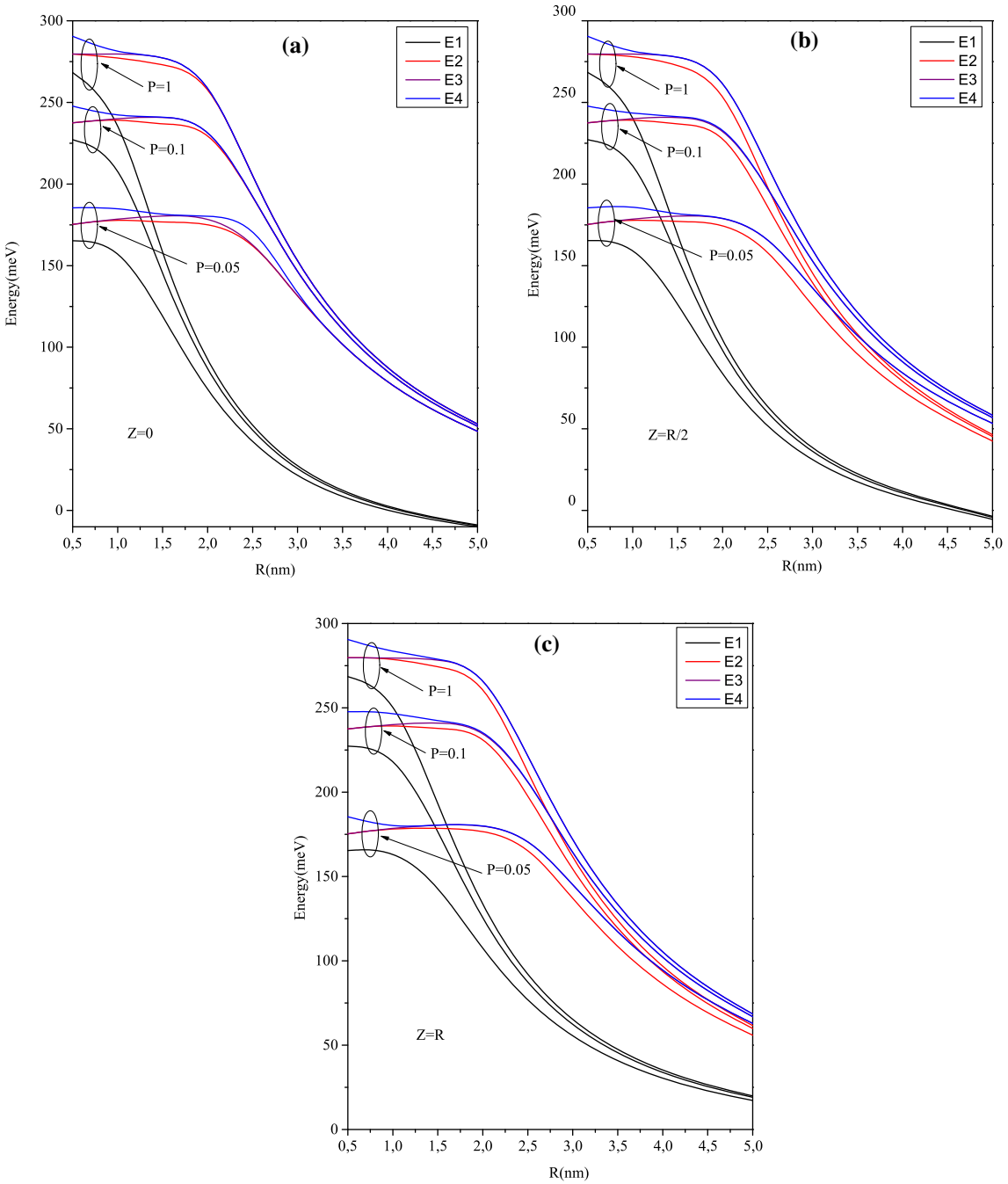


Fig. 5 Ground and excited state energies as functions of the radius of the quantum dot, R, for three values of P ($P = 0.05,\ 0.1,\ 1$) in the cases Z $= 0$ (**a**), Z $= R/2$ (**b**), and Z $= R$ (**c**)

Density plots in Figs. 3 and 4 show the features of wave functions of the lowest four energy states in the system for two different values of the dot radius, R. Figure 3 contains the case where $Z = 0$, and Fig. 4 shows the results when the impurity position has moved to $Z = R$. In Fig. 3, we observed the symmetry of the electron density cloud as the impurity is located at the center of the sphere. We also noticed that the electron density is equally distributed along the quantum dot for the excited states. In Fig. 4, the electron density is found to be shifted toward the edge for the ground and first excited state as the impurity is present at $Z = R$. In the first case, one may see that the symmetries are only slightly perturbed by the Coulombic force of impurity effect. But the vertical displacement of the donor center toward the upper edge noticeably modifies the shape of states. In any case, this can be better appreciated for excited levels.

Changing the value of exponential potential parameter P, Fig. 5 presents plots of the variation of ground and first three excited energy levels as functions of the QD radius, R. First, one readily observes—for all cases depicted—the otherwise expected decreasing

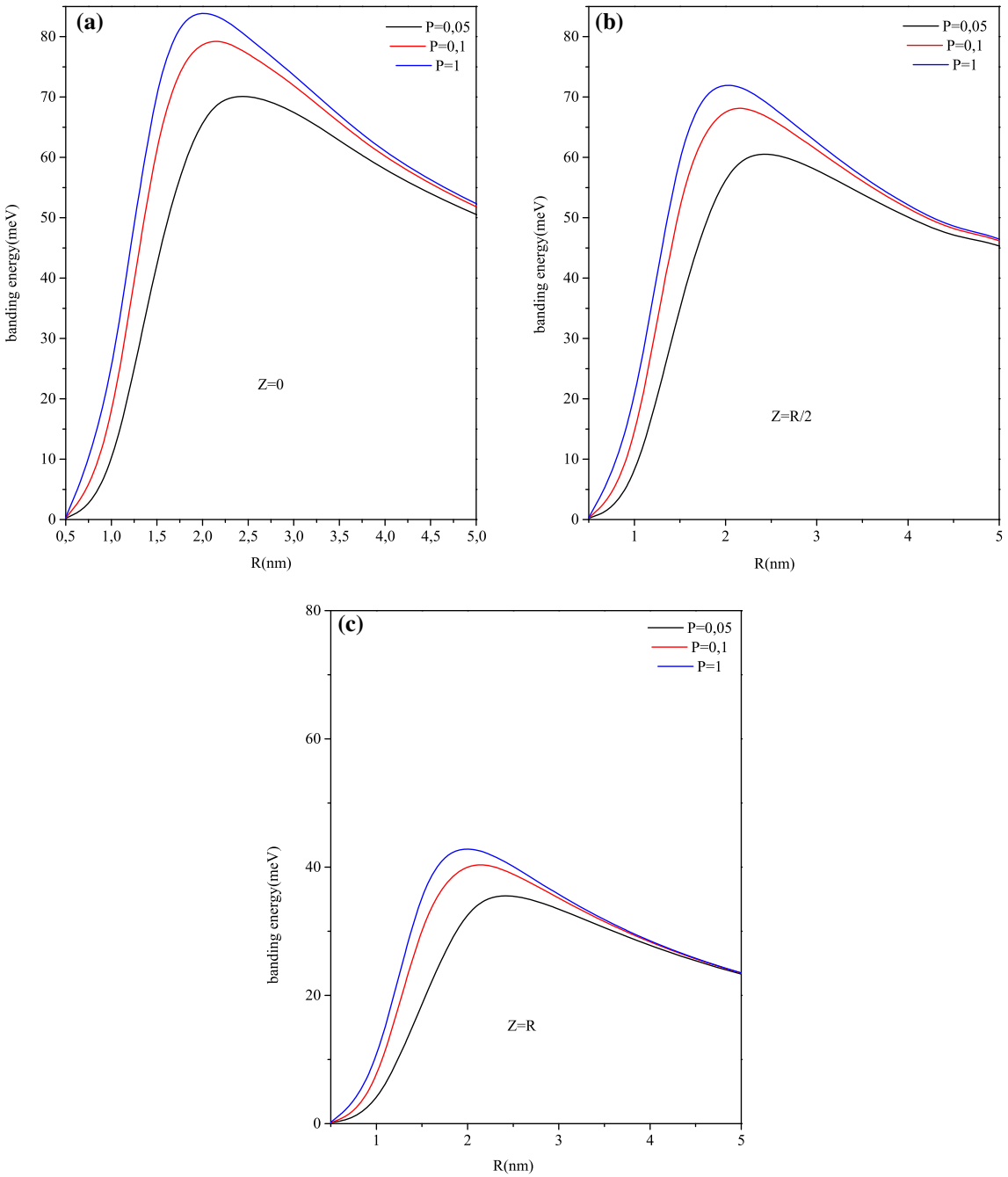


Fig. 6 Binding energy as a function of the radius of the quantum dot, R, for three values of P ($P = 0.05,\ 0.1,\ 1$) in the cases with Z = 0, Z = $R/2$, and Z = R

behavior for larger R, as a consequence of the reduction in spatial carrier confinement. It is also immediately apparent to the effect of augmenting P, which rises the energies of all levels, indicating the increment in particle localization due to the stronger degree of confinement. The Coulomb field intensity has little impact on the degeneracy breaking when the impurity is placed at $Z = 0$, mainly for the smallest and larger values of R. However, when the impurity goes upward to $Z = R/2$ and $Z = R$, a clear separation between the levels can be seen for large enough R, although the proximity between E_1 and E_2 remains when the QD radius is sufficiently small.

The calculated ground state impurity binding energy (BE) appears in Fig. 6 as a function of R, with the same configurations of $V_w(r)$ and impurity position considered before. As noticed, this quantity has an initial increment toward a maximum value whose position shifts to smaller R when P increases. This is understandable if one bears in mind that BE is proportional to the strength of Coulombic interaction between electron and impurity which augments when the confinement is larger. That is, when R increases,

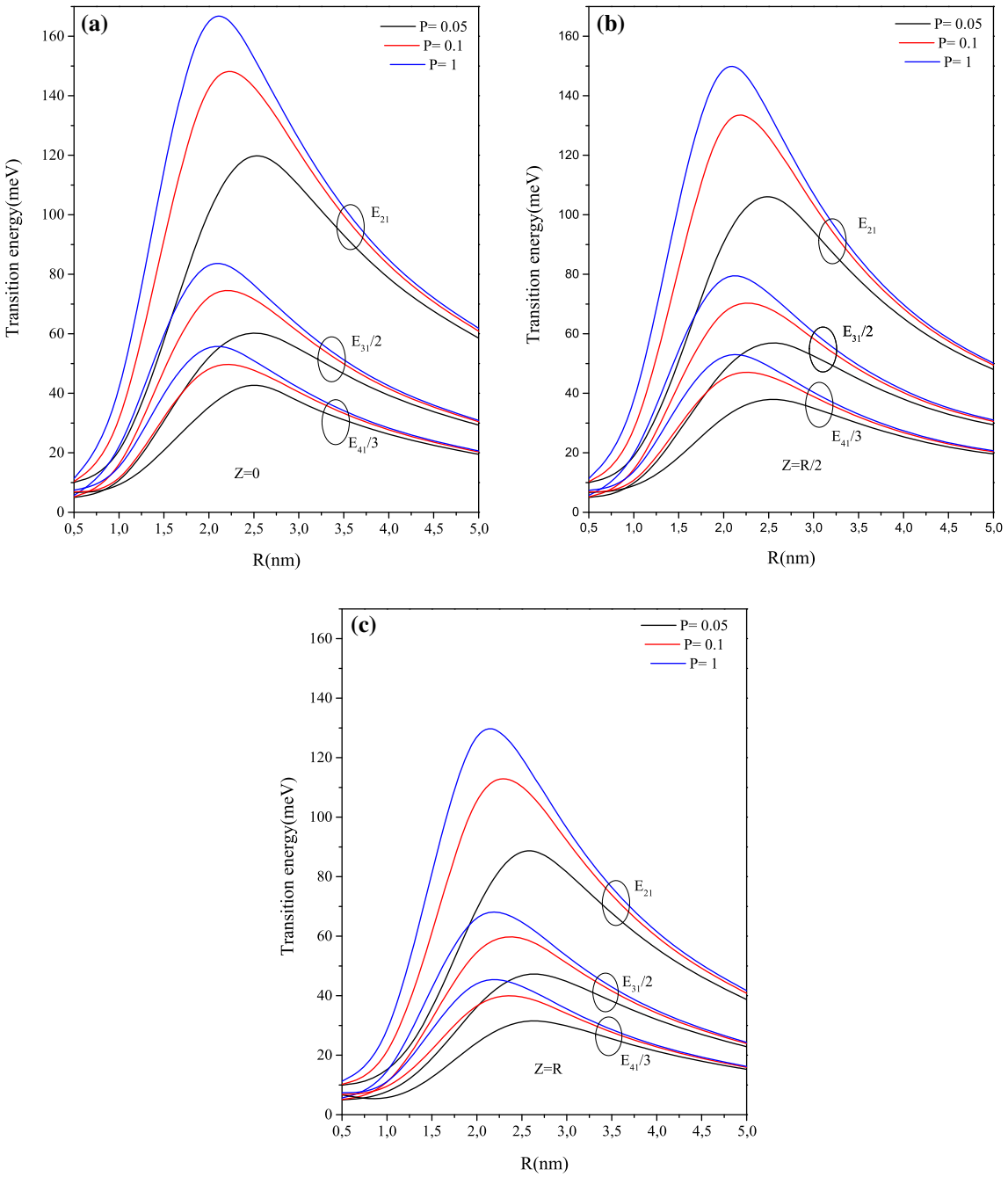


Fig. 7 Transition energies as functions of the radius of the quantum dot, R, for three values of P ($P = 0.05,\ 0.1,\ 1$) in the cases with $Z = 0$, $Z = R/2$, and $Z = R$

the electron-impurity distance tends to diminish, which can be compensated with stronger confinement (greater P). The appearance of a maximum indicates that for a given P, there is a geometrical QD configuration—that depends on the impurity location—at which the electrostatic coupling is the greatest possible. The reduction in BE for larger radii has to do with the reduction in electron spatial localization and the subsequent enlargement of the carrier-impurity distance. Notice, as well, that shifting the donor position away from the dot center implies smaller values of BE, due to the same aforementioned situation.

For the purpose of analyzing the optical responses related to states of the electron-impurity complex, it is of critical relevance to the knowledge of transition energies between allowed levels. These quantities are plotted in Fig. 7 as functions of the QD radius, R, for distinct values of P and different positions of the donor atom. They correspond to electron transition between the ground and the first three excited states. It is possible to observe that the influence of Coulombic coupling makes the shape of the corresponding

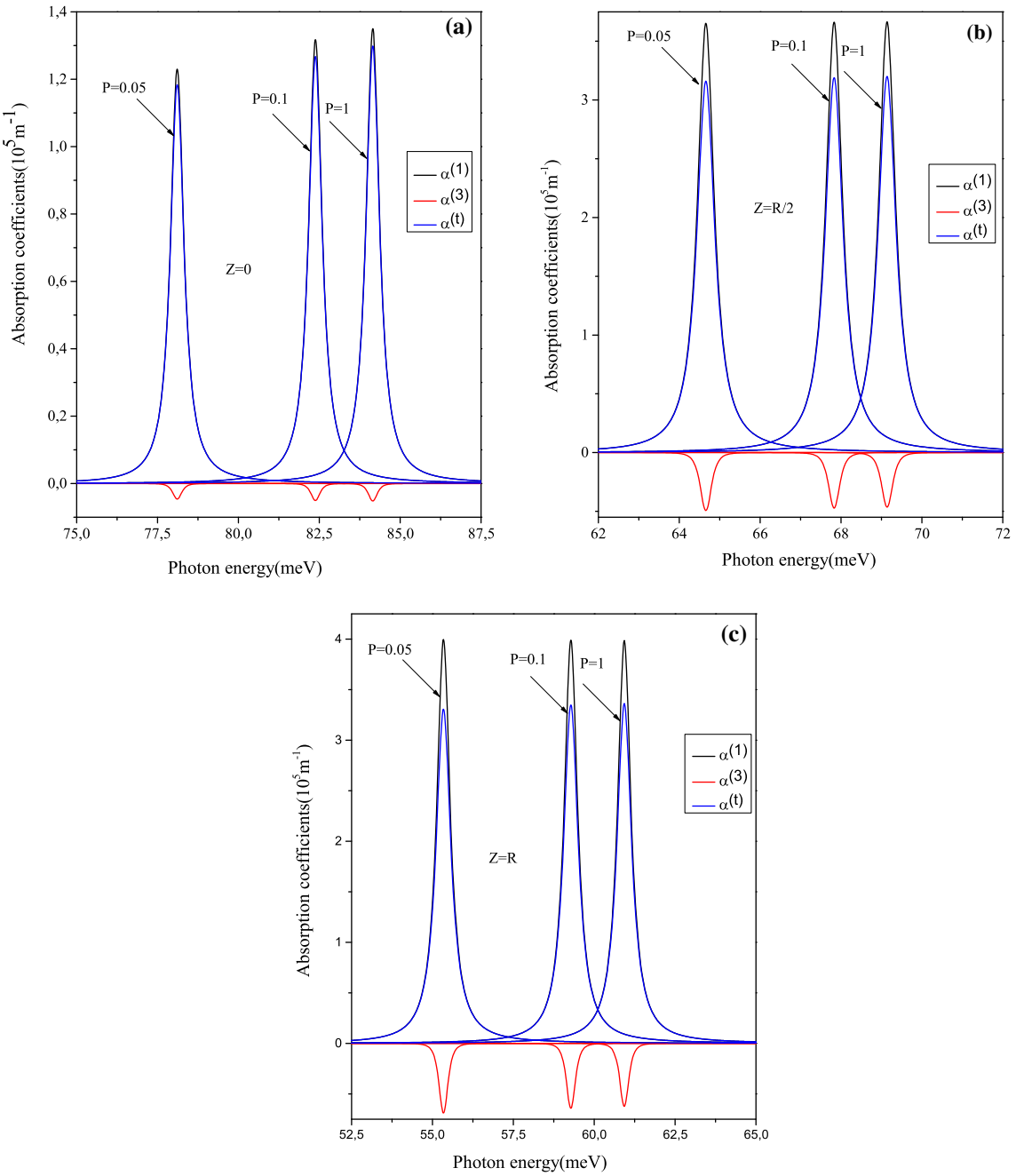


Fig. 8 Optical absorption coefficients (linear, third-order nonlinear, and total) as functions of the incident photon energy, for three values of P ($P = 0.05,\ 0.1,\ 1$) in the cases with $Z = 0$, $Z = R/2$, and $Z = R$

curves resemble the behavior of BE rather than one of the E_i electron levels shown in Fig. 5. Also, there is a similar trend as compared to BE regarding the effect of Z values.

In Fig. 8, we show the calculated linear, nonlinear, and total OAC—related to the electron transition between the ground and the first excited state—as functions of incident photon energy. Again, three different values of the exponential parameter, P, are considered as well as the three—previously mentioned—positions for the impurity: $Z = 0$, $Z = R/2$, and $Z = R$. As expected, the nonlinear contribution is just a fraction of the linear one. But it is worth noticing the effect of impurity shifting from the center on the increment in the relative weight of the—negative—third-order correction. This points to a significant degree of internal polarization that reflects in both the diagonal and off-diagonal parts of the dipole moment matrix. On the other hand, it is readily apparent that the increase in P produces a blueshift of the absorption signal. This is compatible with results for the involved transition energy, E_{10}, shown in Fig. 7. In addition, it is worth highlighting that according to those very results, it verified the existence of an overall shift to lower energies (redshift) of the optical response when the donor location departs from the QD center.

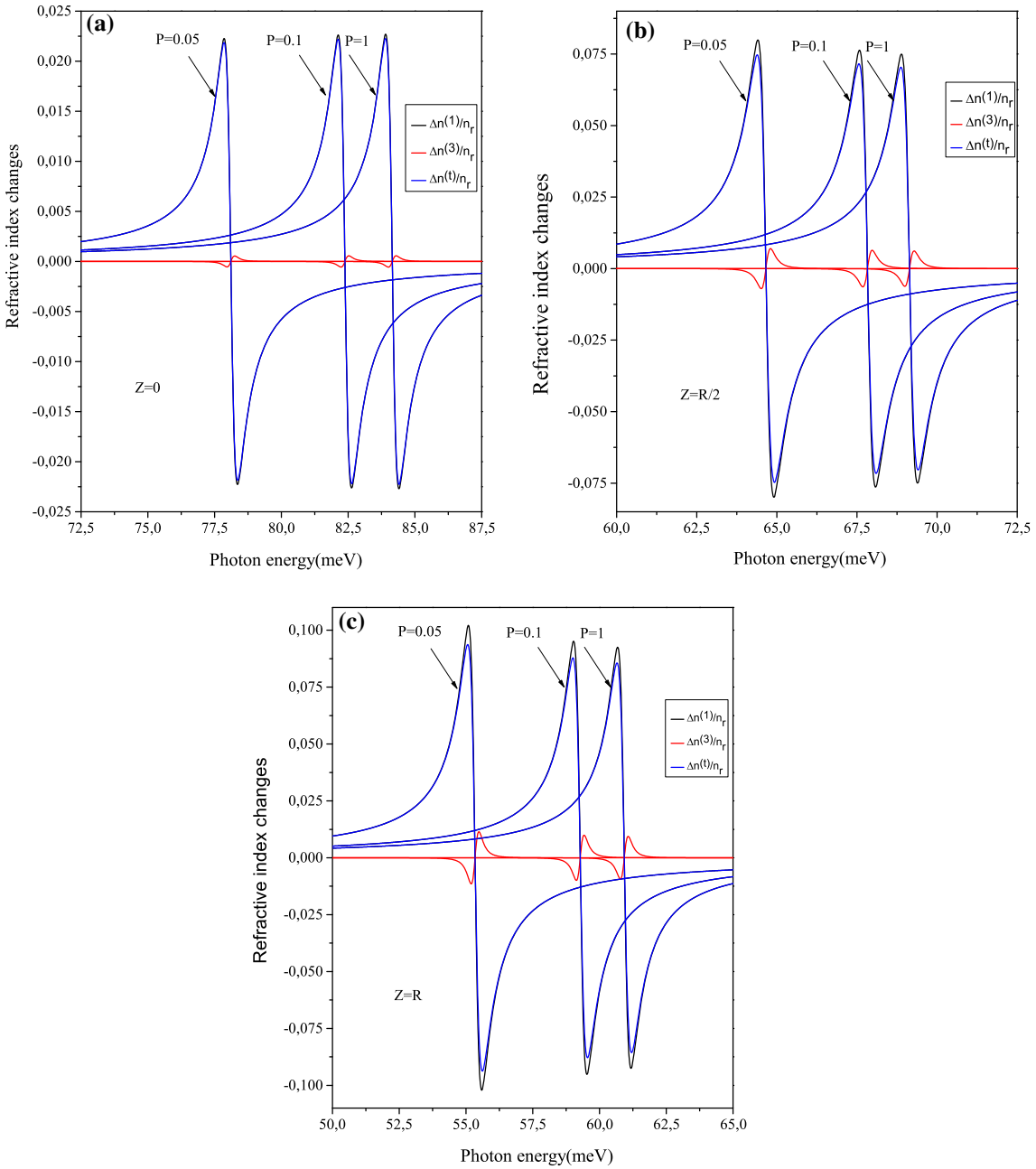


Fig. 9 Coefficients (linear, third-order nonlinear, and total) of the relative refractive index change as functions of the incident photon energy, for three values of P ($P = 0.05,\ 0.1,\ 1$) in the cases with Z = 0, Z = $R/2$, and Z = R

Figure 9 contains the results for calculated RIC, under the same setup used to evaluate the OAC. Here, similar conclusions with respect to signal peak positions can be reached, taking into account the features of inter-state transition energies. However, in this case, it becomes clearer the influence of donor center displacement along the vertical axis, concerning electric polarization. From Eq. (17), it is straightforward that the amplitude of RIC would heavily rely on the value of off-diagonal dipole matrix element M_{10}. Then, according to the pictures in Fig. 9, the shift of Z from 0 to R increases the magnitude of M_{10}.

Coefficients of SHG and THG appear plotted as functions of incident photon energy in Figs. 10 and 11, respectively. It can be observed the same kind of blueshift discussed for the OAC and RIC when values of the exponential parameter P augment. With exception of the $Z = 0$ case, the SHG resonant peak amplitudes have small changes when going from lower to higher values of P. However, it is significant that the height of main SHG resonant peaks undergoes an increment in amplitude when the impurity location moves away from the center. This indicates that the above-mentioned increment in electric polarization leads to an increase in the magnitude of the product of dipole moment matrix elements involved. The opposite happens in the case of THG. From Fig. 11, it is clear that all peak amplitudes reduce when the location of the donor center shifts toward the QD edge. In this situation, it can

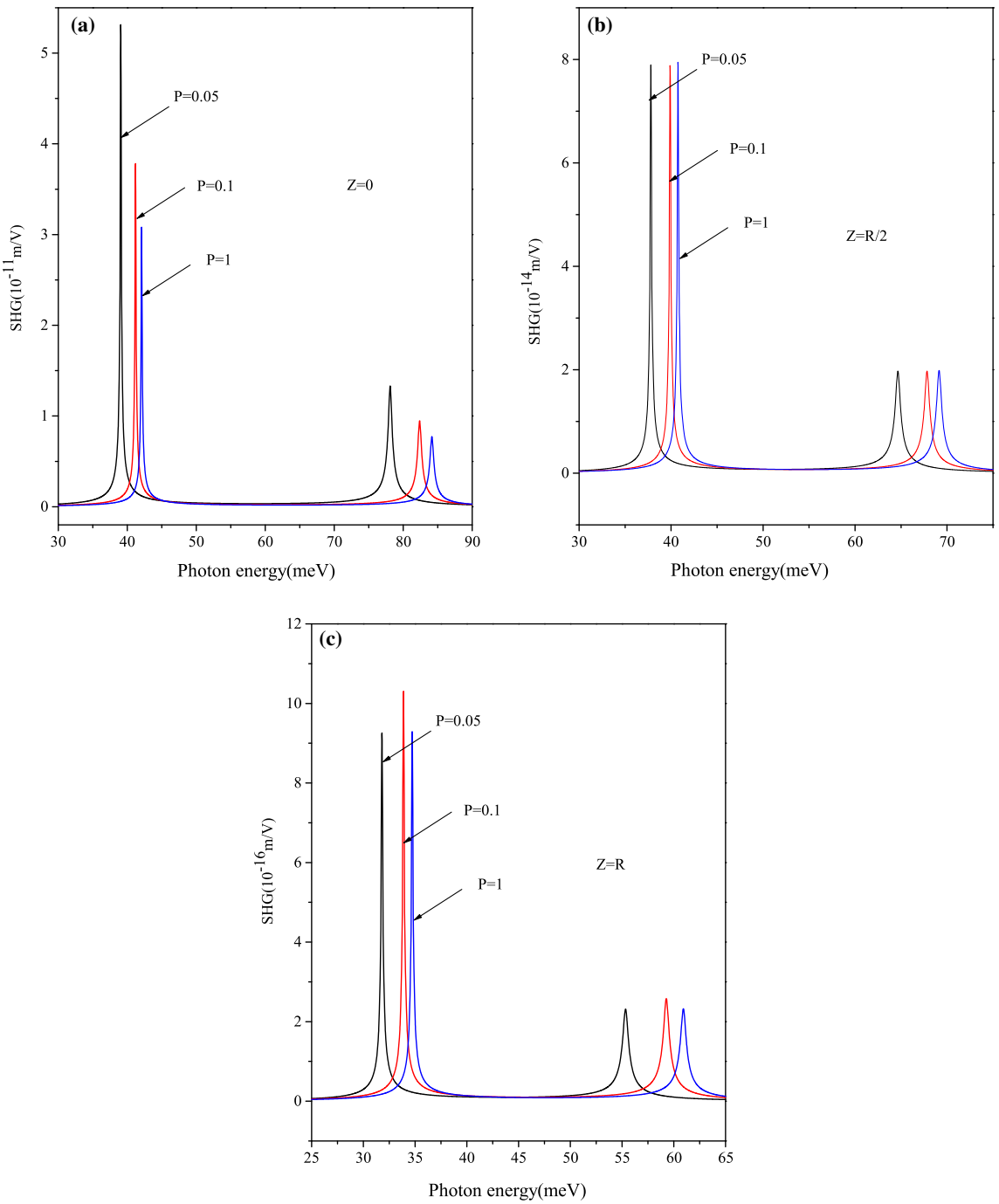


Fig. 10 Coefficient of second harmonics generation as a function of the incident photon energy, for three values of P ($P = 0.05,\ 0.1,\ 1$) in the cases with $Z = 0$, $Z = R/2$, and $Z = R$

be concluded that the magnitude of the factor $M_{23}\ M_{30}$ suffers a noticeable reduction, which can be attributed to the particular spatial distribution of probability densities associated with the second and third excited states, ψ_2 and ψ_3. That is, the corresponding overlapping between these wavefunctions is so that the associated dipole moment elements are larger when the impurity is at the dot center or sufficiently close to it. The overall redshift, previously commented, is also noticed for both SHG and THG coefficients, being more apparent when $Z = R/2$.

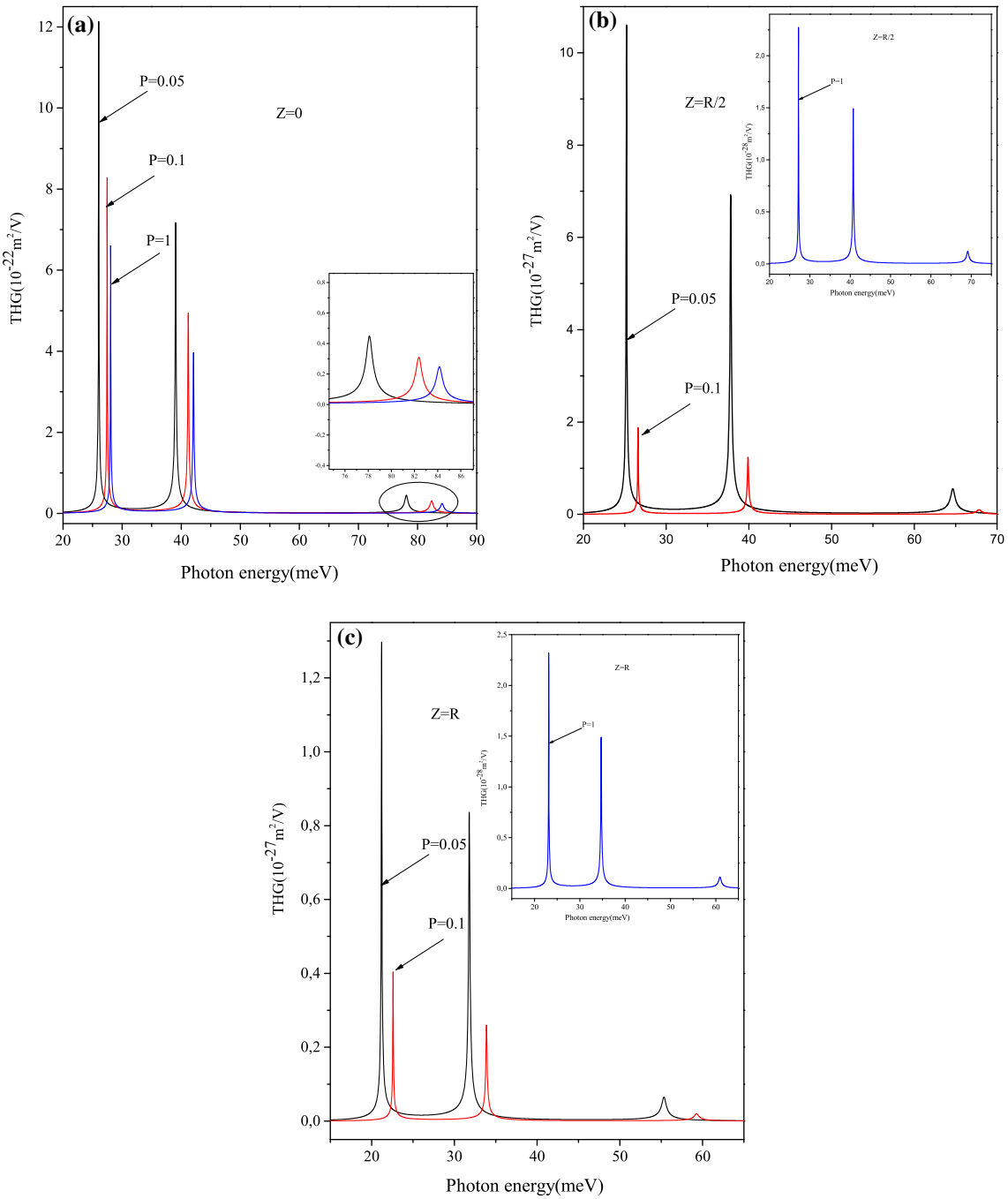


Fig. 11 Coefficient of third harmonics generation as a function of the incident photon energy, for three values of P ($P = 0.05,\ 0.1,\ 1$) in the cases with $Z = 0$, $Z = R/2$, and $Z = R$

4 Conclusion

We have investigated the optical properties of spheroid SiGe/Si QD in power-exponential potential using finite element method with the presence of hydrogenic impurity. The position of the impurity plays imperative role in the optical properties as this changes the electron density orientation and the energy of the system. The potential parameter controls the optical response as blueshift is observed in all optical properties with increase in P. As the impurity shifts from center to toward the edge then a redshift is observed in all optical properties, i.e., optical absorption coefficient, relative refractive index changes, second harmonic generation, and third harmonic generation peaks. The understanding of these nonlinear optical properties will serve as a literature for modeling and tuning the optical properties of optoelectronic devices.

Acknowledgements L. M. Pérez acknowledges financial support from ANID through Convocatoria Nacional Subvención a Instalación en la Academia Convocatoria Año 2021, Grant SA77210040. D. Laroze acknowledges partial financial support from Centers of Excellence with BASAL/ANID financing Grant AFB180001, CEDENNA. M. E. Mora-Ramos acknowledges support from Mexican CONACYT through Grant A1-S-8218 (CB 2017-2018).

Author's contribution All the authors contributed equally to the manuscript.

Data Availability Statement This manuscript has associated data in a data repository. [Authors' comment: The datasets generated during and/or analyzed during the current study are available from the corresponding author on reasonable request.].

References

1. A.I. Ekimov, A.A. Onushchenko, JETP Lett. **34**, 345–349 (1981)
2. A.I. Ekimov, A.A. Onushchenko, Sov. Phys. Semicond. **16**, 775–778 (1982)
3. M.A. Kastner, Phys. Today **46**, 24 (1993)
4. R. Ashoori, Nature **379**, 413–419 (1996)
5. T. Chakraborty, in *Nanoscopic quantum rings: A new perspective*, vol 43. ed. by B. Kramer. In Advance in Solid State Physics (Springer: Berlin/Heidelberg, 2003), pp. 79–94.
6. B. Krishan, M.R. Garg, Int. J. Adv. Res. Electr. Electron. Instrum. Eng. **4**, 7857 (2015)
7. A.L. Efros, Nature **575**, 604–605 (2019)
8. G. Cantele, D. Ninno, G. Iadonisi, Calculation of the infrared optical transitions in semiconductor ellipsoidal quantum dots. Nano Lett. **1**, 121 (2001)
9. L.C.L.Y. Voon, M. Willatzen, Confined states in lens-shaped quantum dots. J. Phys. Condens. Matter. **14**, 13667 (2002)
10. R.J. Warburton, C. Schulhauser, D. Haft, C. Scheflein, K. Karrai, J.M. Garcia, W. Schoenfeld, P.M. Petroff, Phys. Rev. B **65**, 113303 (2002)
11. H. Lee, H.C. Leventis, S.J. Moon, P. Chen, P.S. Ito, S.A. Haque, T. Torres, F. Nesch, T. Geiger, S.M. Zakeeruddin, M. Grätzel, Md.K. Nazeeruddin, Adv. Funct. Mater. **19**, 2735 (2009)
12. A. Oukerroum, E. Feddi, J. Bosch Bailach, J. Martinez-Pastor, F. Dujardin, E. Assaid, J. Phys. Condens. Matter **22**, 375301 (2010)
13. M. Sabaeian, A.K. Nasab, Appl. Opt. **51**, 4176 (2012)
14. M. Sabaeian, M. Riyahi, Physica E **89**, 105 (2017)
15. M.C. Lbl, S. Scholz, I. Sllner, J. Ritzmann, T. Denneulin, A. Kovcs, B.E. Kardynal, A.D. Wieck, A. Ludwig, R.J. Warburton, Commun. Phys. **2**, 1 (2019)
16. C. Heyn, A. Radu, J.A. Vinasco, D. Laroze, R.L. Restrepo, V. Tulupenko, N.N. Hieu, H.V. Phuc, M.E. Mora-Ramos, J.H. Ojeda, A.L. Morales, C.A. Duque, Opt. Laser Technol. **139**, 106953 (2021)
17. M. Kria, Varsha, M. Farkous, V. Prasad, F. Dujardin, L. M. Perez, D. Laroze, E. Feddi, Curr. Appl. Phys. **25**, 1–11 (2021)
18. F.Y. Huang, Y.S. Tang, J.N. Duan, K.L. Wang, Electron. Lett. **33**, 1736–1737 (1997)
19. M.R. Sakr, H.W. Jiang, E. Yablonovitch, E.T. Croke, Appl. Phys. Lett. **87**, 223104 (2005)
20. W.M. Witzel, R. Rahman, M.S. Carroll, Phys. Rev B **85**, 205312 (2012)
21. V. Kornich, Ch. Kloeffel, D. Loss, Quantum **2**, 70 (2018)
22. Ch. Volk, A. Chatterjee, F. Ansaloni, Ch.M. Marcus, F. Kuemmeth, Nano Lett. **19**, 5628–5633 (2019)
23. E.J. Connors, J.J. Nelson, H. Qiao, L.F. Edge, J.M. Nichol, Phys. Rev. B **100**, 165305 (2019)
24. Th. McJunkin, E.R. MacQuarrie, L. Tom, S.F. Neyens, J.P. Dodson, B. Thorgrimsson, J. Corrigan, H. Ekmel Ercan, D.E. Savage, M.G. Lagally, R. Joynt, S.N. Coppersmith, M. Friesen, M.A. Eriksson, Phys. Rev. B **104**, 085406 (2021)
25. A.R. Mills, Ch.R. Guinn, M.J. Gullans, A.J. Sigillito, M.M. Feldman, E. Nielsen, J.R. Petta, Sci. Adv. **8**, eabn5130 (2022)
26. E.J. Connors, J. Nelson, L.F. Edge, J.M. Nichol, Nat. Commun. **13**, 940 (2022)
27. R.W. Boyd Nonlinear Optics, 2nd edn. (Academic Press) (2003)
28. K.G. Dvoyan, D.B. Hayrapetyan, E.M. Kazaryan, A.A. Tshantshapanyan, Nanoscale Res. Lett. **2**, 601 (2007)
29. L. Lu, W. Xie, Z. Shu, Phys. B Condens. Matter **406**, 3735 (2011)
30. S.G. Nobandegani, M.J. Karimi, Opt. Mater. **82**, 75 (2018)
31. M.R.K. Vahdani, G. Rezaei, Phys. Lett. A **373**, 3079 (2009)
32. A. El Aouami, M. Bikerouin, K. Feddi, N. Aghoutane, M. El-Yadri, E. Feddi, F. Dujardin, A. Radu, R.L. Restrepo, J.A. Vinasco, A.L. Morales, C.A. Duque, M.E. Mora-Ramos, Philos. Mag. **100**, 2503 (2020)
33. V.V. Nautiyal, P. Silotia, Phys. Lett. A **382**, 2061 (2018)
34. B. Li, K.X. Guo, C.J. Zhang, Y.B. Zheng, Phys. Lett. A **367**, 493 (2007)
35. I. Karabulut, S. Baskoutas, J. Compt. Theo. Nano. **6**, 153 (2009)
36. M. Kirak, Y. Altinok, Eur. Phys. J. B **85**, 344 (2012)
37. M. Varsha, J.. El. Kria, L.M. Hamdaoui, V. Pérez, M. Prasad, D. Laroze. El-Yadri, M. El Feddi, Nanomaterials **11**, 1513 (2021)
38. C.Y. Lin, Y.K. Ho, J. Phys. B At. Mol. Opt. Phys. **45**, 145001 (2012)
39. K.L. Jahan, b. Boyacioglu, and A. Chatterjee, Scientific Reports, 9, 15824(2019)
40. W. Xie, Superlattices Microstruct. **65**, 271 (2014)
41. J.L. Liu, J. Zhu, J. Appl. Phys. **101**, 093709 (2007)
42. V. Prasad, P. Silotia, Phys. Lett. A **375**, 3910 (2011)
43. Varsha, P. Silotia and V. Prasad, AIP Conf. Proc., 2220, 020154(2020)
44. M.R.K. Vahdani, G. Rezaei, Phys. Lett. A **374**, 637 (2010)
45. I.S. Ruddock, Eur. J. Phys. **15**, 53 (1994)

Springer Nature or its licensor (e.g. a society or other partner) holds exclusive rights to this article under a publishing agreement with the author(s) or other rightsholder(s); author self-archiving of the accepted manuscript version of this article is solely governed by the terms of such publishing agreement and applicable law.